Separation and Purification Technology 233 (2020) 115989

Contents lists available at ScienceDirect

Separation and Purification Technology

journal homepage: www.elsevier.com/locate/seppur

Polyaniline@porous polypropylene for efficient separation of acid by diffusion dialysis

Pradeep K. Prajapati[a,b,d], Naresh N. Reddy[a,c,d], Raghavendra Nimiwal[a], Puyam S. Singh[b,d], S. Adimurthy[c,d], Rajaram K. Nagarale[a,d,*]

[a] Electro Membrane Processes Division, CSIR-Central Salt and Marine Chemicals Research Institute, Bhavnagar 364002, India
[b] Membrane Science and Separation Technology Division, CSIR-Central Salt and Marine Chemicals Research Institute, Bhavnagar 364002, India
[c] Natural Products & Green Chemistry Division, CSIR-Central Salt and Marine Chemicals Research Institute, Bhavnagar 364002, India
[d] AcSIR, CSIR-Central Salt and Marine Chemicals Research Institute, Bhavnagar 364002, India

ARTICLE INFO

Keywords:
Acid separation
Diffusion dialysis
Polyaniline
Polypropylene

ABSTRACT

Herein we have discussed the robust design and synthetic methodology of polyaniline based exceptional chemical and mechanical stable composite membrane for acid recovery by diffusion dialysis. Physicochemical characterization of the membrane was carried out to find its hydrophilic/hydrophobic characteristic and its effect on separation of HCl and H_2SO_4 from the simulated solution. The high retention of sulfuric acid or high permeation of HCl was explained on the basis of Gibbs free energy of hydration of Cl^- and SO_4^{2-} ions. The obtained diffusion coefficient (U_H^+) for PANI and A-PANI membrane was in the range of 0.013–0.042 m h^{-1} for HCl, H_2SO_4 and effluent solution. The maximum acid recovery was 43% for A-PANI and 32% for PANI. The acid recovery for locally available effluent solution was ~34% indicating potential use of synthesized membranes in acid recovery by diffusion dialysis.

1. Introduction

Polyaniline (PANI) belongs to a class of conducting polymer with excellent chemical and thermal stability [1–3]. It can be prepared by chemical or electrochemical oxidation in aqueous as well as organic medium with excellent yield, controlled molecular weight and at a different level of doping. A π-conjugated structure of PANI is an excellent ion transporter [4,5] and its efficacy depends on molecular weight, morphology and Donnan potential [6]. Emeraldine form of PANI has been well studied for protonation with different anions and it was found that bulkier the anion, lower the conductivity [7] due to low permeability through closely packed polymer chains [7,8]. In the presence of electric gradient, the conductivity is due to concerted shifting of protons accompanied by electrons across the polymer chain. But in the absence of electric gradient, transfer of proton can be obtained by concentration gradient across the film and this property can be utilized for acid separation by diffusion dialysis [9,10]. Sufficient number of reports are available on composite membrane preparations, where powdered PANI has been physically blended with engineering polymers like polystyrene [11] and PVDF [12] to make functional membranes as proton exchange and/or anion exchange [13–16]. The use of anion exchange membranes is wide spread. It is used in separation/purification of inorganics/organics by electro dialysis [17], as a membrane separator in alkaline fuel cell [18], Zn/bromide redox flow battery [19] and acid recovery by diffusion dialysis [20]. The generalized preparation methodology of anion exchange membrane includes chloromethylation followed by amination of engineering thermoplastics like, polystyrene, Polyethersulfone, polyether ether ketone etc. [21]. The chloromethylation step involves the use of highly carcinogenic chloro-methyl methyl ether. So there are huge efforts to make anion exchange membrane by alternative methods like, use of nitrogen based heterocycles, or alkyl bromination followed by amination [18,21]. These membranes have been successfully used in acid recovery by diffusion dialysis [20]. However they exhibited low proton permeability due to dense and symmetric microstructure [22,23]. The high proton permeability i.e. proton diffusion coefficient (U_H^+) of 0.043 m h^{-1} have been reported with thin film composite [24]. Herein, we have rationally designed new membranes with excellent chemically stability and good acid diffusion ability. The membranes were designed and prepared without use of chloro-methyl-methyl ether, a highly carcinogenic chemical. It composed of microporous polypropylene support to provide desired mechanical strength and polyaniline over layer which acts as sieving and proton transporting medium for effective separation of acid. Though there are reports on composite of PANI

* Corresponding author at: Electro Membrane Processes Division, CSIR-Central Salt and Marine Chemicals Research Institute, Bhavnagar 364002, India.
E-mail address: rknagarale@csmcri.res.in (R.K. Nagarale).

https://doi.org/10.1016/j.seppur.2019.115989
Received 2 July 2019; Received in revised form 8 August 2019; Accepted 26 August 2019
Available online 27 August 2019
1383-5866/

Nomenclature

Abbreviations

APS	ammonium persulphate
A-PANI	poly(o-anisidine)
DMF	N,N,dimethylformamide
DD	diffusion dialysis
MWCO	molecular weight cut-off
OPA	orthophosphoric acid
PANI	polyaniline
PE	polyethylene
PEG	polyethylene glycol
PEO	polyethyleneoxide
PP	polypropylene
PVA	polyvinyl alcohol
PVDF	poly(vinylidine fluoride)
TMA	trimethylamine
BPPO	bromo methylated poly(2,6-dimethyl-1,4-phenylene oxide)
QPPO	quaternized poly(2,6-dimethyl-1,4-phenylene oxide)
TEMED	N,N,N′,N′-tetramethylethylene diamine

Symbols

M_C	mass of coated sample
M_{NC}	mass of uncoated sample
M_w	weight of wet sample
M_d	weight of dry sample
C_f	concentration of feed
C_p	concentration of permeate
r_p	pore radius
S	separation factor
U	dialysis coefficient
M	moles of salute transported per hour
A	effective area
ΔC	logarithmic average concentration between two chambers
C_f^0	feed concentration at initial time
C_f^t	feed concentration at time, t
C_d^t	dialysate concentration at time, t
U_{H^+}	proton diffusion coefficient
$U_{Fe^{3+}}$	Fe^{3+} diffusion coefficient

with cross-linked polystyrene [25], polycarbonate [26], polypropylene [27], polyethylene [28] and polyamide [29], their use in acid separation has not been reported.

2. Experimental

2.1. Materials

Ammonium persulphate (APS), methanol, aniline and polyvinylalcohol (Avg. Mw, 1,25,000) were purchased from SD fine chemicals, Mumbai, India. Orthophosphoric acid (OPA), N, N-dimethylformamide (DMF), Sulphuric acid (H_2SO_4) were obtained from SRL chemicals, Mumbai, India. Trimethylamine (TMA) was received from Fisher scientific, India. Polypropylene (PP) sheet i.e. battery separator having 60 μM thickness was obtained from M/s Targray Technology International Inc., Canada. Deionized water (DI) was used for all of the experiments.

2.2. Methods

2.2.1. Synthesis of polyaniline and poly(o-anisidine) membrane at PP support

Polyaniline (PANI) and Poly(o-anisidine) (A-PANI) membranes were synthesized by contra-diffusion process over the microporous PP substrate. Prior to synthesis, PP substrate was soaked in 30 mL DMF followed by the addition of 20 mL PVA solution (1 wt%) with 5 mL aniline/o-anisidine for the surface activation and pre-treatment of the substrate. After the pre-treatment of 3 h, the substrate was mounted between two chambers of contra-diffusion cell.[10] Separately, 2 mL aniline was slowly mixed in freshly prepared 3.5 M H_2SO_4 (500 mL) solution and stirred to get transparent solution, termed as solution-A. Similarly 4 g of APS was dissolved in another 500 mL solution of 1 M H_2SO_4 designated as solution B. Both solutions A and B were filled in the two separate chambers of cross-diffusion cell consisting activated PP support. Both solutions were continuously circulated for 5 h in the cell by using peristaltic pump with flow rate of 30 mL/min to carry out the polymerization reaction at the interface of PP sheet and aniline solution. After completion of the reaction, membrane was removed from the cell and washed several times with DI water to remove unreacted molecules from the membrane. The obtained membrane was designated as PANI membrane and it was stored in water. Similar procedure was followed for the synthesis of A-PANI membrane where o-anisidine was used in above synthesis process instead of aniline. These membranes were designated as A-PANI membrane. The chemical reactions involved in membrane synthesis are depicted in Scheme 1.

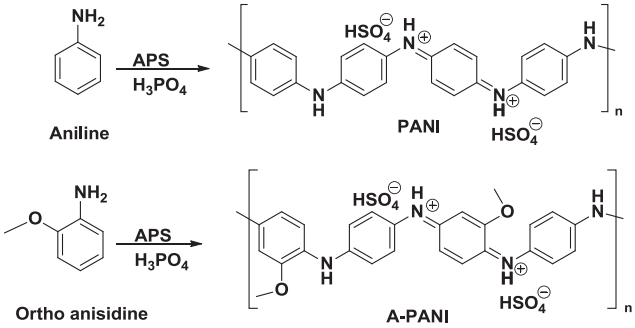

Scheme 1. Synthesis reaction scheme of polyaniline (PANI) and o-anisidine (A-PANI) membrane.

2.2.2. Membrane characterization

The surface morphology and structural analysis of the synthesized membranes were thoroughly characterized using various analytical tools. Contact angle measurement (water) were performed on goniometer, DSA 100 Krüss GmbH instrument, Germany. Membrane surface roughness and topology was recorded in semi-contact mode with Atomic Force Microscopy (AFM) using AFM instrument (Ntegra Aura, NT-MDT, Moscow). The chemical functionalities were analysed by Fourier-transform infrared-attenuated total reflectance (FTIR-ATR). The spectra were recorded on Agilent, Cary 600 series FTIR microscope, (with a resolution of ± 4 cm^{-1} and incident angle of 45°) in the wavenumber range of 400–4000 cm^{-1}. Membrane surface morphology was scanned on Field emission-scanning electron microscope (FE-SEM) using JEOL JEM 7100F, USA coupled with energy-dispersive X-ray (EDX) spectroscopy at an accelerating voltage of 15–20 kV. The thermal characteristics of the membrane was analysed using thermo gravimetric analysis (TGA), TA instruments 2960 (METTLER TOLEDO, Germany), at a heating rate of 10 °C min^{-1} from 30 to 800 °C in the N_2 atmosphere.

2.2.3. Coating density and water content measurement

Coating density of the synthesized PANI and A-PANI membrane was measured by quantitative analysis. Coating density (%) was calculated using the following equation,

$$Coating\ density\ =\ \left(\frac{M_C - M_{NC}}{M_{NC}}\right) \times 100 \quad (1)$$

where M_C represents the mass of the coated membrane and M_{NC} is the mass of the uncoated PP substrate. Membrane samples with specific area of 8.55 cm^2 were cut and dried in oven at 60 °C for certain time till the constant weight was achieved. The final weight values were used for the calculation of coating density.

Water content of the synthesized membranes was calculated by gravimetric method, measuring the weight gain of the membrane. Firstly the membranes were cut into specific area of 4 cm^2 and kept in water to calculate the mass of the wet membrane (M_w). Afterwards these membrane samples were transferred in the vacuum oven for drying at 60 °C to get constant dry weight (M_d). These weight values were used to calculate water content using the following equation,

$$Water\ content\ (\%)\ =\ \left(\frac{M_w - M_d}{M_d}\right) \times\ 100 \quad (2)$$

2.2.4. Pure water flux, solute rejection and pore radius measurement

The water permeability and solute rejection experiments were performed on lab scale testing kit containing a testing cell with booster pump to apply the upstream pressure. Distilled water was supplied as feed solution for testing the water permeability of the membranes. A circular membrane sample having an effective membrane area of 15 cm^2 was mounted on the test cell and upstream pressure of 3–5 bar was applied. The membranes were stabilized for 1 h before considering the water flux measured value. Pure water permeability (PWP) was calculated using the following equation.

$$PWP = \frac{Q}{A} \quad (3)$$

where Q ($Q = v/t$) is the water flux at permeated side (lh^{-1}), and A represents an effective membrane area (m^2).

PEG (0.4, 9 and 35 kDa) and PEO (100 and 200 kDa) of different molecular weights, which have different stock radii of 0.47, 1.16, 5.68, 8.98 nm calculated using the relation for PEG $a = 16.73 \times 10^{-10} M^{0.557}$ and for PEO = $10.44 \times 10^{-10} M^{0.587}$ [30]. Where, 'a' represents the Stokes radius and M is the molecular weight of PEG and PEO.

The known Stokes radii PEG/PEO were passed through the membranes at applied pressure of 3 bar. The MWCO values were obtained from the molecular weight vs. rejection profile (Fig. 7) where the MWCO values at 90% rejection of the solute was measured for PANI and A-PANI membranes. The concentration of feed (C_f) and permeate (C_p) samples were analysed by the Gel Permeation Chromatography (GPC) using Analytical Technologies Ltd. Instrument. The rejection values (R%) were calculated using the following equaiton [31]

$$R(\%) = \left(1 - \frac{c_p}{c_f}\right) \times 100 \quad (4)$$

The obtained R% data was used to calculate the MWCO of the membranes. The pore radius (r_p) of the membranes were calculated by using MWCO values in Eq. (5) [32].

$$r_p\ =\ 0.045 \times MWCO^{0.44} \quad (5)$$

2.2.5. Acid and iron diffusion studies

Acid diffusion of PANI and A-PANI membranes in batch mode were studied using two compartment diffusion cell with an effective area of 4.2 cm^2 (Fig. 1). Equal volume of 250 mL DI water was filled at one side while 250 mL acid solution was filled in other side. The solution of both compartments were re-circulated using the peristaltic pumps and amount of acid diffused into the water compartment was estimated by acid base (NaOH) titration using phenolphthalein indicator. The change in concentration of iron was measured using UV–visible spectrophotometer with ammonium thiocyanate reagent. The effluent was collected from local bentonite industry with composition ~3.5 M acid and 5–6% iron content. Usually it is the mixture of H_2SO_4, HCl and HNO_3. But amount of H_2SO_4 is dominated. Apart from this it has the metal ion impurities like, Mo, Cu, Zn, Cr, Mn, Mg, Ca etc. The acid diffusion coefficient (U_{H^+}) was calculated using following formula [33].

$$U = \frac{M}{At\Delta C} \quad (6)$$

where M, represents the moles of proton transported across the membrane, t shows the time (h), A is the active area (m^2) of the membrane and ΔC represents the logarithmic average concentration among the both compartments of the diffusion cell defined in mole/m^3. It can be calculated by Eq. (7), using initial feed concentration (C_f^0) at time 0, feed concentration (C_f^t) after time 't' and dialysate concentration (C_d^t) at time t [22,23,33]. It should be noted that ($C_f^0 - C_d^t - C_f^t$) ≠ 0, because of water transport across the membrane resulted volume change in the cell chambers [34,35].

$$\Delta C = \frac{(C_f^0 - C_d^t - C_f^t)}{\ln\left[\left(C_f^0 - C_d^t\right)/C_f^t\right]} \quad (7)$$

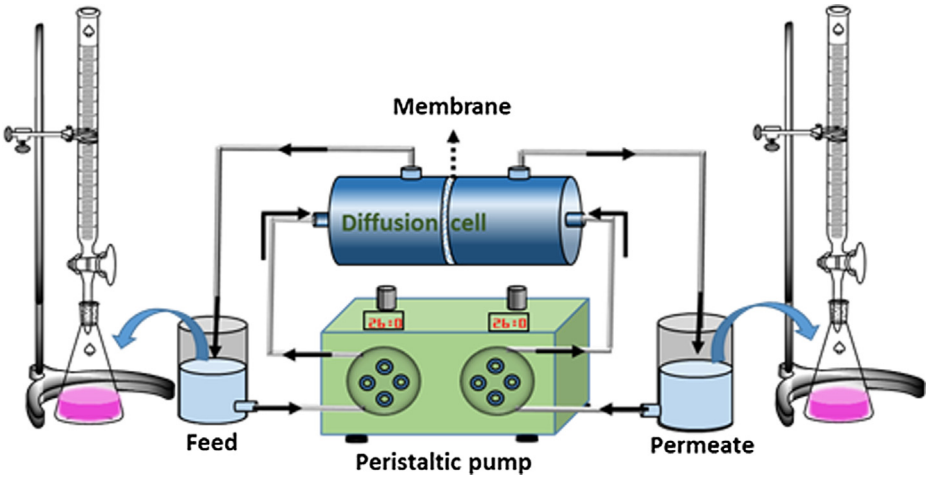

Fig. 1. Schematic of experimental setup for acid diffusion study.

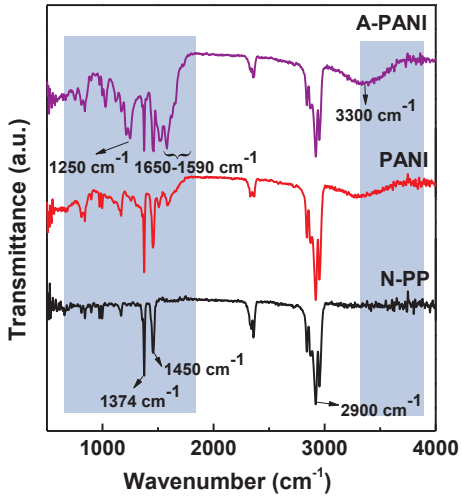

Fig. 2. FTIR-ATR spectra of N-PP, PANI and A-PANI membranes.

Table 1
Coating density, water content and average pore size of N-PP, PANI and A-PANI membranes.

Membranes	Coating density (%)	Water content (%)	Pore size (nm)
N-PP	–	–	~500
PANI	9.50	31.10	4.27
A-PANI	29.10	90.60	3.72

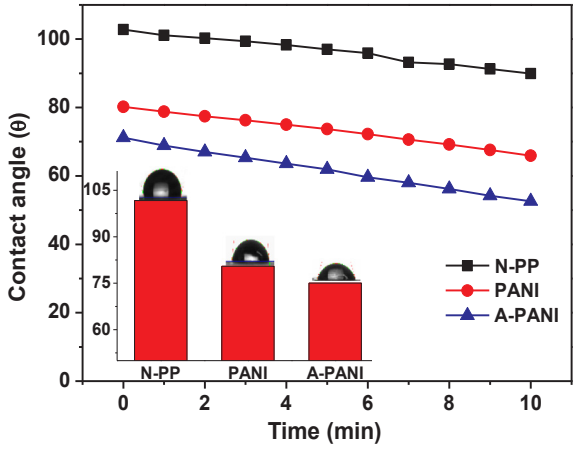

Fig. 3. Contact angle (water) measurement of N-PP, PANI and A-PANI membranes in static (inset) and dynamic mode at 10 min time duration.

3. Results and discussion

3.1. Membrane synthesis

PANI and A-PANI were successfully synthesized on the porous PP substrate by chemical oxidation of aniline and o-anisidine using APS as an oxidizing agent under the similar experimental conditions. High coating density was observed for A-PANI membranes due to electron donating −O−CH_3 group, which facilitates the polymerization reaction. The formation of PANI and A-PANI membranes at PP substrate was indicated by change in colour of white PP sheet into dark green colour.

3.2. Characterization of membranes

3.2.1. FTIR-ATR spectroscopy

The analytical techniques were used to confirm the membrane formations. In the infrared spectra of PP substrate, PANI and A-PANI membranes, the strong absorption bands at ~1374 cm^{-1} and 1450 cm^{-1} were assigned to C−H bending mode of CH_3 and CH_2 groups while ~2900 cm^{-1} band corresponds to C−H stretching of CH_2 groups of PP backbone [36,37] (Fig. 2). The appearance of new absorption peaks at ~1650–1590 cm^{-1} along with broad absorption peak at ~3300 cm^{-1} corresponds to N−H bending and stretching mode of secondary amines, confirming the successful formation of PANI [38]. Absorption peaks at low IR region (~690–900 cm^{-1}) belongs to aromatic C−H bending mode of out of plane [39]. A-PANI membranes exhibited a broad absorption band at ~3300 cm^{-1} with higher intensity than PANI membrane. The change in band intensity corresponds to O−H (absorbed moisture) and N−H stretching of A-PANI membrane. [40] A new absorption peak at ~1250 cm^{-1} belongs to C−O stretching of O−CH_3 group of A-PANI membrane [39]. A-PANI membranes exhibited a broad absorption band at ~3300 cm^{-1} with higher intensity than PANI membrane. The change in band intensity corresponds to O−H (absorbed moisture) and N−H stretching of A-PANI membrane [40].

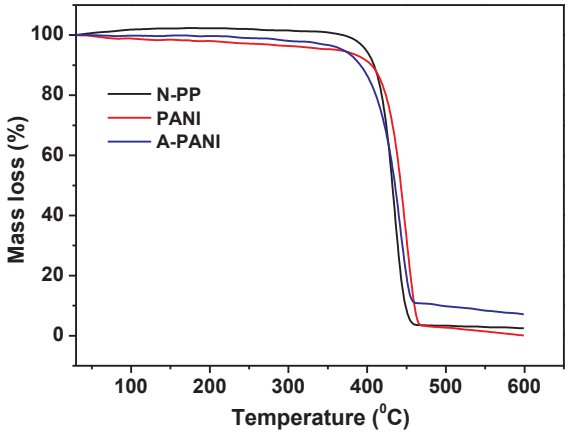

Fig. 4. TGA analysis of N-PP, PANI and A-PANI membranes membranes.

3.2.2. Coating density, contact angle and water content measurement

The coating density of synthesized PANI and A-PANI polymer was calculated by measuring the polymer amount coated over the PP substrate. The highest coating density of 29% was observed for A-PANI membranes followed by PANI membranes with low coating density of 9.5% as given in Table 1. The high coating density of A-PANI is attributed to its high degree of polymerisation due to electron donating effect of −O−CH_3 group, which results into formation of high molecular weight polymer chains and hence the high coating density. Coating density can be directly related to the surface characteristics of the membrane, contact angle, surface roughness etc. The measured contact angles (CA) of the membranes can give information about its hydrophilic characteristic (Fig. 3). Contact angle controls by solid-gas interface tension ($\gamma_{s,a}$), solid–liquid interface tension ($\gamma_{s,l}$) and liquid-gas interface tension ($\gamma_{l,a}$) based on Young's equation, $Cos\ \theta = (\gamma_{s,a} - \gamma_{s,l})/\gamma_{l,a}$. Usually, on increasing the surface roughness, CA value tends to decrease [40]. The membranes with CA value of less than 90° considers as hydrophilic membranes. The Measured CA values for N-PP, PANI and A-PANI were ~101°, ~80° and ~75°, respectively. The dynamic CA measurement of the membranes exhibited 22, 19 and 26% decrease for N-PP, PANI and A-PANI, respectively. The 26% decrement in CA of A-PANI membranes was in accordance with its hydrophilic nature. The gravimetric water content of the membrane were measured and presented in Table 1. The higher water content of ~90% was observed for A-PANI membrane followed by PANI membrane with ~31% water uptake as shown in Table 1. The high water content of the coated membranes is due to presence of free water in pores of the

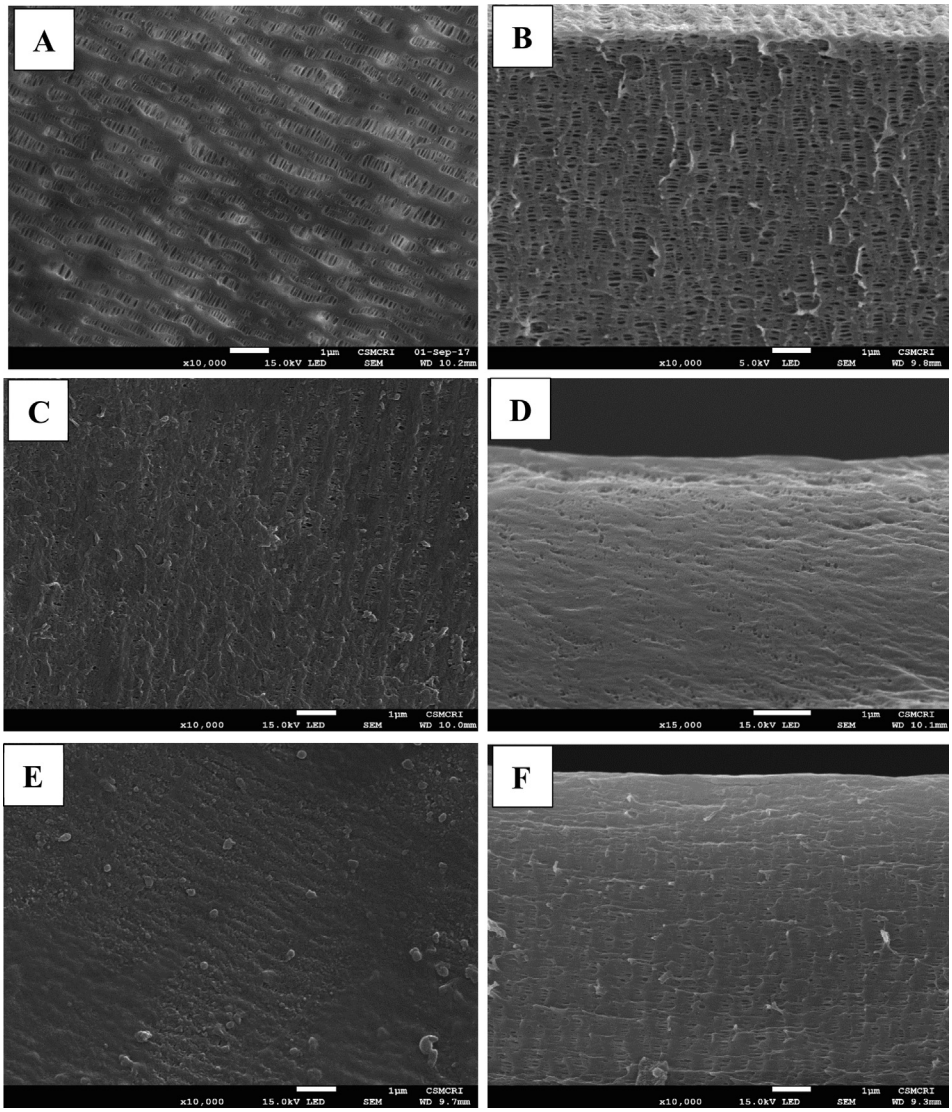

Fig. 5. SEM images of membrane surface (A, C and E) and cross-section images (B, D and F) of N-PP, PANI and A-PANI membranes respectively.

membranes. They were in accord to coating density. However, N-PP membrane did not show any water content because of its hydrophobic behaviour.

3.2.3. TGA analysis

The thermal stabilities of the membranes were analysed under the N_2 atmosphere shown in Fig. 4. The N-PP started degradation at ~380 °C and ended at ~460 °C in a single step where 90% weight loss was observed. The degradation of PANI was started at ~380 °C and completed at ~460 °C with 90% weight loss [38]. The initiation of degradation of A-PANI was started ~370 °C and completed at ~470 °C with 80% weight loss. The low temperature of initiation of degradation of A-PANI than PANI indicates its poor thermal stability. The mechanism of degradation of these polymers will be similar to as reported [41,42]. Usually it is associated with the loss of protonic acid component of the polymer followed by loss of gasses like acetylene and ammonia.

3.2.4. SEM and AFM analysis

The membranes morphology was analysed by surface and cross-section SEM images. Fig. 5A and B shows the surface and cross-section image of N-PP support showing highly porous microstructure with average surface pore size of ~500 nm. After in-situ synthesis of PANI, partial pore filled structure was observed. The coating was uniform without aggregation and/or phase separation. The smooth surface was clearly visible in surface as well as cross-section images Fig. 5C and D. From the SEM images of A-PANI membranes (Fig. 5E and F), pore of N-PP was completely filled on the surface. But cross section images shows partial filling, indicating the polymerisation of o-anisidine mostly occurred on the interface of solution and PP sheet. Whereas polymerisation of aniline occurred throughout PP membrane phase. This is due to the high degree of polymerisation of o-anisidine, promoted by highly electron donating $-O-CH_3$ group. The method of membrane preparation was by contra-diffusion method, where solution from the both compartment compete with each other to diffuse into the PP sheet. In case of PANI, the simultaneous diffusion of the solution starts polymerisation deep into the PP sheet matrix. Whereas in case of A-PANI, before diffusion of o-anisidine solution into the PP matrix, it comes in contact with APS solution at interface where growth of A-PANI starts. Fig. 6 shows the AFM images of N-PP, PANI and A-PANI membranes. The scanning area of specimen was 10X10 μM. The measured average roughness and peak to peak distance values for all membranes are presented in Table 2. Smooth and uniform surface with lowest roughness and peak to peak distance values of 13.34 nm and 164.40 nm was observed for commercial N-PP support. With polymerisation of aniline, the roughness was increased to 21.05 nm and peak to peak distance was

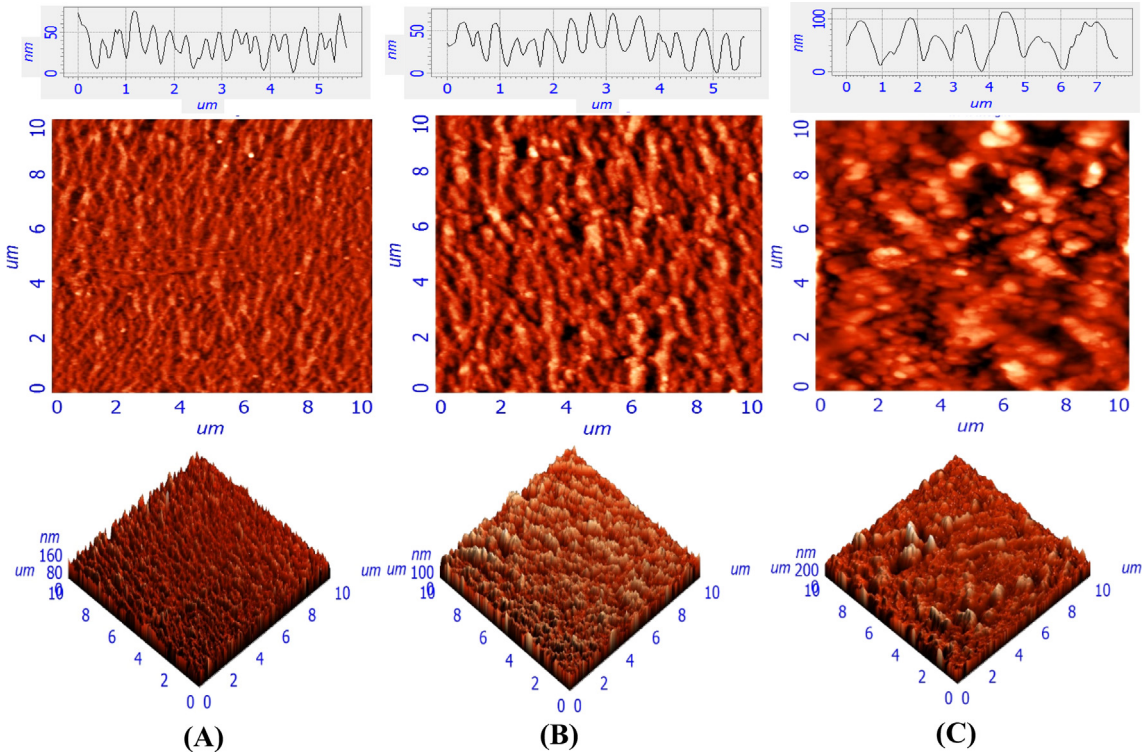

Fig. 6. Atomic force microscopy images of average roughness and surface topology along with surface-depth profile of (A) N-PP, (B) PANI and (C) A-PANI membranes.

Table 2
Surface roughness statistical parameters analysed by AFM analysis of the membranes.

Statistical Parameters (nm)	N-PP	PANI	A-PANI
Peak to peak, Sy	164.40	233.70	351.00
Mean Value	68.42	130.24	170.55
Roughness Average, Sa	13.34	21.05	36.00
Root mean square, Sq	16.21	25.98	45.46

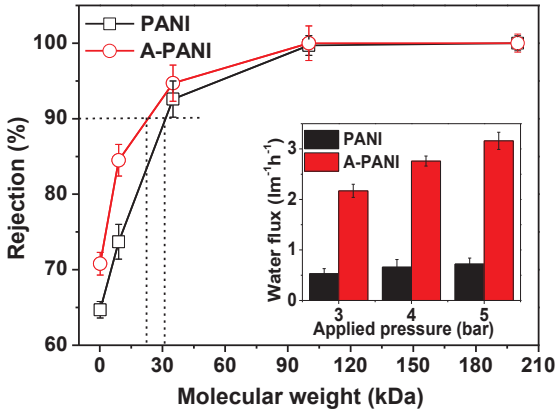

Fig. 7. Solutes (PEG and PEO) rejection, molecular weight cut-off and pure water flux of N-PP, PANI and A-PANI membranes.

233.70 nm. Furthermore, polymerisation of o-anisidine results into further increase in roughness and peak to peak distance values of 36.00 nm and 351.00 nm respectively. The highly rough and heterogeneous surface of A-PANI was due to the formation of high molecular weight polymer. The surface-depth profile of all three membranes were analysed and shown with AFM images. The nodular sizes of polymer was found in increasing order of N-PP < PANI < A-PANI as observed from their depth profiles. Surface- depth profiles were acquired by simple section analysis from horizontal direction of the image using Nova P9-Ntegra software. The results were in agreement with SEM images on the basis of coating density of the polymer.

3.2.5. Pure water permeability and MWCO study

Since the membranes were synthesized by in-situ polymerisation, deep intrusion of the polymer into PP matrix was evident by surface morphology and topology examined by SEM and AFM analysis. However, water permeability and MWCO experiments were conducted to study the overall performance of the membrane. The water flux experiments were performed on cross-flow testing cell by applying upstream pressure in range of 3–5 bar. The water flux was measured for every hour keeping the equilibrium time of half an hour to achieve steady state after changing the upstream pressure. The water flux experiments were repeated at least three times in order to get average water flux values and results are depicted in Fig. 7 (inset). PANI membranes exhibited average water flux of 0.53–0.72 $l\,m^{-2}\,h^{-1}$, which was lower than the obtained water flux of 2.17–3.16 $l\,m^{-2}\,h^{-1}$ for A-PANI membranes. The low water permeability of PANI membranes was due to its coating deep into the PP matrix and its water content. The inclusion of PANI deep into the PP matrix blocks the pores of PP sheet effectively. It results into the nearly dense or nanoporous membrane and hence the low water flux. Whereas, coating of A-PANI was observed only on the surface of PP sheet (SEM images, Fig. 5) which results into the open pores of the PP sheet. The thin barrier top coated layer followed by microporous substructure, and more hydrophilic membrane character results into higher water flux for A-PANI membranes.

The MWCO values were determined by plotting the rejection (R %) versus molecular weight (*Mw*) of different solutes as shown in Fig. 7. PANI membranes exhibited lower rejection profile than A-PANI membranes for PEG 0.4, 9 and 35 kDa. The rejection for PEO 100 and 200 kDa was observed > 99% for both PANI and A-PANI membranes. The *Mw* corresponding to 90% rejection was determined from the

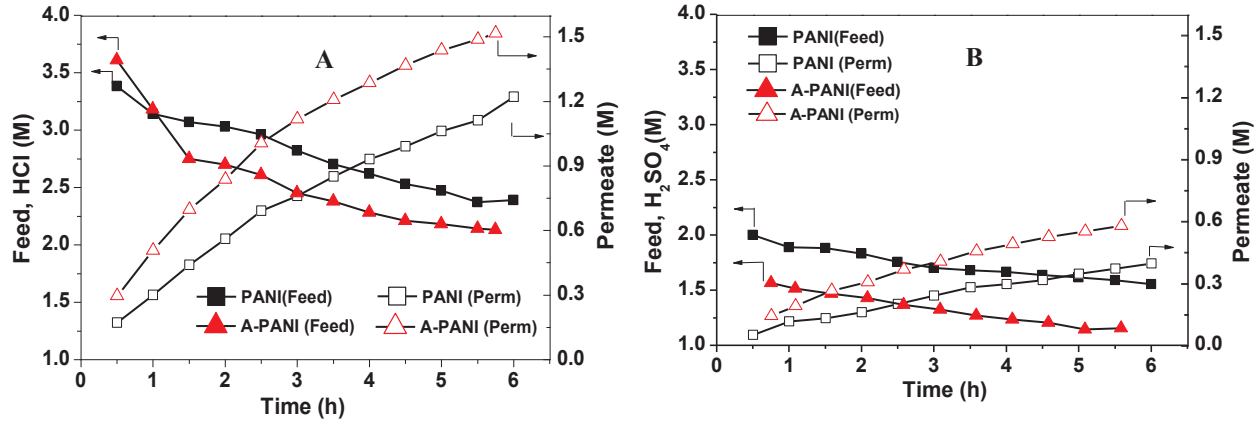

Fig. 8. Acid diffusion results from HCl and H_2SO_4 acid solutions using PANI and A-PANI membranes with time.

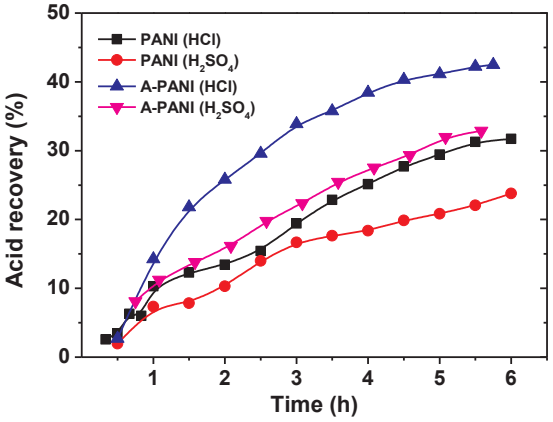

Fig. 9. Acid recovery (%) from HCl and H_2SO_4 acid solutions using PANI and A-PANI membranes with time.

crossover point of rejection values. The obtained MWCO values of 31 and 22 kDa were used in Eq. (5) and the average pore radius (r_p) of PANI and A-PANI membranes were found to be 4.2 nm and 3.7 nm, respectively. The smaller pore radius of A-PANI membrane was explained based on its high coating density obtained from higher degree of polymerization of o-anisidine than the PANI membrane.

3.3. Diffusion study of acid and iron

The acid diffusion study was performed in two compartment cell in a batch mode. The solution in both compartments was continuously recirculated at constant flow rate as shown in Fig. 1. The initial experiments were performed with known concentration of HCl and H_2SO_4, without metal ions to evaluate the membrane's preferential transport. Because the industrial effluent contains the mixture of acids. Fig. 8 shows the change in concentration of feed and permeate compartment with time. The concentration of feed compartment was decreased whereas permeate compartment was increased. The maximum concentration obtained at permeate side was 1.5 M for A-PANI membrane and 1.2 M for PANI membrane when, ~3.5 M HCl was used as feed solution (Fig. 8A). The higher flux of A-PANI membrane despite of low pore size was explained on the basis of different pore characteristics. Generally, the pores can be classified into closed pore, blind pore and through pores. In case of A-PANI because of its only surface polymerisation, the membrane may be dominated by through pores. But in case of PANI, which polymerises deep into the PP matrix, membrane pores dominated by the closed or blind pores results into the low flux. SEM cross-section images of the membranes clearly visualise the differences. Further, high hydrophilicity and water content of the A-PANI is responsible for high flux of acid. When we changed the feed solution to H_2SO_4, the maximum acid recovery was 0.4 and 0.6 M in a 6 h experiment for PANI and A-PANI membranes respectively (Fig. 8B). This corresponds to 33.5 and 24.0% H_2SO_4 recovery with respect to initial feed concentration for A-PANI and PANI membrane respectively. The percent of HCl recovery was 43.0 and 32.0% for A-PANI and PANI membrane respectively (Fig. 9).

The high HCl recovery compare to H_2SO_4 is explained on the basis of Gibbs Hydration Energy of Cl^- and SO_4^{2-} anions [43,44]. The measurement of Gibbs free energy ($-\Delta G_h^o$ (kJ/mol)) states that higher the value, the stronger the hydration of anion. The reported Gibbs free energy for Cl^- and SO_4^{2-} anions were 317 and 1000 kJ/mol respectively, indicating stronger hydration of SO_4^{2-} anion, the hydration number was 16 [44] whereas hydration number of Cl^- ion was 8 [45]. This suggests that the sulphate ions are bulky and hydrophilic compared with chloride ions, it is reasonably self-explained that the hydrophilic ions are difficult to permeate through the hydrophobic membranes. In the present study, A-PANI is more hydrophilic compare to PANI (Fig. 4, contact angle measurements) hence it has high acid recovery. Compare to HCl and H_2SO_4, it has high HCl recovery. Fig. 10(A) and (B) shows the acid recovery with simulated solution, consisting of 5% $FeCl_3$ and 3.5 M HCl, and effluent solution obtained from local bentonite mines. The acid recovery with PANI membrane was 27%, whereas A-PANI membrane showed 37% acid recovery, ~10% higher. It is due to its relatively hydrophilic nature, high water content and through pores membrane structure. It showed maximum acid recovery with effluent solution was ~35%

(Fig. 10(A)). PANI membrane showed extremely low acid recovery i.e. ~17%. Fig. 10(C) and (D) shows the permeation of Fe^{3+} in simulated as well as effluent solution. The permeation was higher for the A-PANI membrane. The maximum permeation was ~0.23 μM. This permeation is far lower than the permeation of proton. The extremely low permeation is due to its high Gibbs free energy of hydration. The reported Gibbs free energy of hydration was 4580 kJ/mole [46]. It corresponds to 16.6 water molecules per ion or hydration number with 0.288 nm ionic radius [46]. These values indicates that Fe^{3+} has relatively higher size and hydrophilic nature and hence it is sluggish to pass through the relatively hydrophobic A-PANI and PANI membranes, hence the low permeability. The calculated Diffusion Coefficient (U_{Fe}^{3+}, m h^{-1}) was presented in Table 3 along with the separation factor. A-PANI has the higher Diffusion Coefficient and lower separation factor compare to PANI for simulated as well as effluent solution. But in comparison to the simulated solution, effluent solution showed higher diffusion coefficient and lower separation factor due to the presence of organic and other metal ions impurities.

The low acid recovery is explained on the basis of its hydrophobic nature and presence of sulphate ion in solution. Also presence of organic foulent in the effluent affects acid recovery naturally. To get the

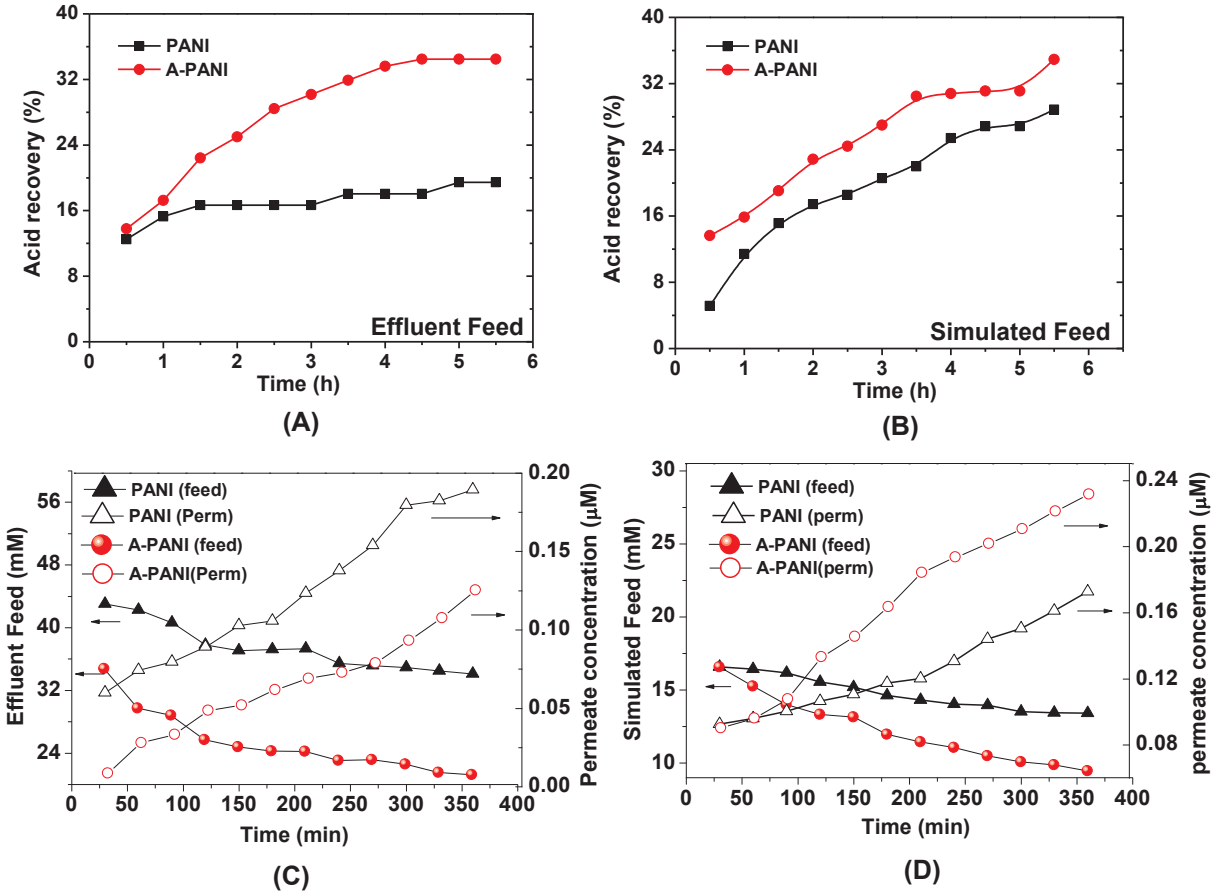

Fig. 10. Acid recovery (%) (A, B) and Fe^{3+} diffusion (C, D) from effluent and simulated solutions using PANI and A-PANI membranes with time.

Table 3
Diffusion Coefficient of Fe^{3+} ions and the separation factor from simulated ($HCl/FeCl_3$) and effluent solution using PANI and A-PANI membranes.

Membranes	Fe^{3+} diffusion ($U_{Fe}{}^{3+}$, $m\,h^{-1}$) $\cdot 10^{-3}$		Separation factor (S)	
	Simulated	Effluent	Simulated	Effluent
PANI	0.747	1.925	19.65	0.806
A-PANI	1.393	4.075	16.90	0.619

further insight on membranes, diffusion coefficient of acid ($U_H{}^+$) was calculated and presented in Fig. 11. They are in accord with the reported values presented in Table 4, along with selectivity. The high $U_H{}^+$ value of $\sim 0.042\,m\,h^{-1}$ was obtained for A-PANI with HCl solution. The low $U_H{}^+$ value of $\sim 0.013\,m\,h^{-1}$ was obtained for PANI membrane with H_2SO_4 solution. The results indicate that PANI@PP sheet offer an alternate membrane material for acid separation by diffusion dialysis in harsh effluent condition.

4. Conclusion

The synthesis of polyaniline and poly(o-anisidine) based membrane was effectively demonstrated on microporous hydrophobic polypropylene sheet by contra diffusion method. The measured contact angle indicated, the PANI membrane was more hydrophobic than the A-PANI membrane. The SEM images, surface view and cross-sectional

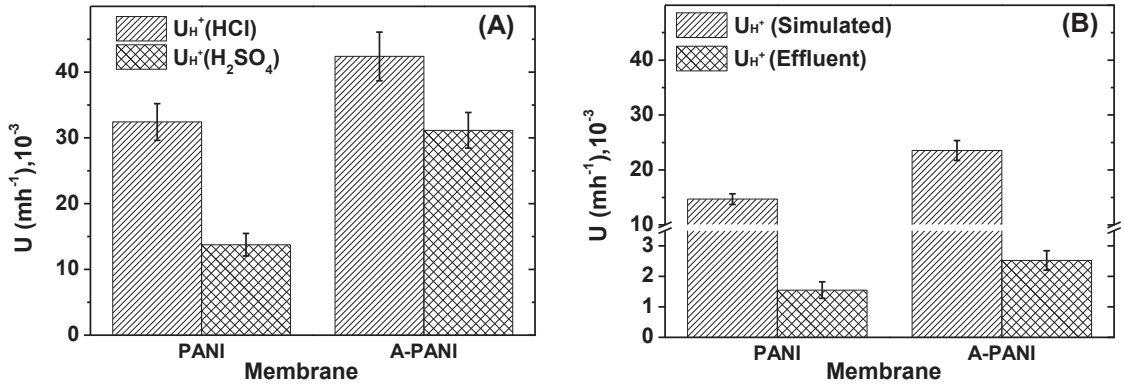

Fig. 11. The study of H^+ diffusion coefficient from, (A) HCl and H_2SO_4 acid solutions and (B) iron containing simulated and effluent feed solutions by using PANI and A-PANI membranes.

Table 4
Comparison of the present study results with some of the published literatures.

Membranes	U_{H^+} (m h^{-1})	Selectivity	References
Quaternized PANI membranes	0.017–0.020	26.42–32.3	[10]
Quaternized PPO based hybrid membrane	0.005–0.011	17–32	[22]
PVA, multi-alkoxy silicon copolymer membranes	0.01–0.017	24–30.1	[23]
BPPO UF membranes modified by TEMED	0.009–0.043	46.6–73.8	[24]
PVA hybrid membrane	0.011–0.018	18.5–21	[32]
PVA treated with alkoxysilane membranes	0.008–0.01	15.9–21	[47]
Quaternized aromatic amine based hybrid PVA membranes	0.017–0.025	14–21	[48]
Electrospun QPPO nanofiber membrane	0.041–0.070	5.62–68.05	[49]
Imidazole based AEM	0.018–0.048	12.72–52.5	[50]
Pore filled AEM	0.18×10^{-3}–0.09×10^{-3}	35.57–40.99	[51]
Modified Neosepta AFX membranes	0.001×10^{-3}–0.062×10^{-3}	11.31–47.65	[52]
PANI	0.032	19.65	Present
A-PANI	0.042	16.90	study

view indicates the polymerization of aniline was throughout the PP matrix whereas o-anisidine polymerization was mostly on surface. The water permeability experiments conclude the formation of 3–4 nm average pore radius of the membrane. The diffusion dialysis experiment performed in HCl and H_2SO_4 solution revealed the high recovery for HCl due to low Gibbs free energy of hydration of Cl^- ion than SO_4^{2-} ion. The maximum acid recovery of 43% for A-PANI and 32% for PANI was obtained. The acid recovery for locally available effluent solution was ~34% indicating potential use of synthesized PANI and A-PANI membranes in acid recovery.

Acknowledgement

RKN thanks for the financial support (grant number EMR/2016/001977) from Science and Engineering Research Board (SERB), DST India. Director CSIR-CSMCRI is acknowledged for continuous support and encouragement. Instrumentation facility provided by Analytical Discipline & Centralized Instrument Facility, CSIR-CSMCRI, Bhavnagar, are gratefully acknowledged. PP thanks for the senior research fellowship (SRF) from CSIR, India. CSIR-CSMCRI manuscript number-053/2019.

References

[1] E. Genies, A. Boyle, M. Lapkowski, C. Tsintavis, Polyaniline: a historical survey, Synth. Met. 36 (1990) 139–182.
[2] S. Bhadra, D. Khastgir, N.K. Singha, J.H. Lee, Progress in preparation, processing and applications of polyaniline, Prog. Polym. Sci. 34 (2009) 783–810.
[3] M. Sairam, S. Nataraj, T.M. Aminabhavi, S. Roy, C. Madhusoodana, Polyaniline membranes for separation and purification of gases, liquids, and electrolyte solutions, Sep. Purif. Rev. 35 (2006) 249–283.
[4] A. MacDiarmid, J. Chiang, A. Richter, Epstein, AJ, Polyaniline: a new concept in conducting polymers, Synth. Met. 18 (1987) 285–290.
[5] H. Reiss, Theoretical analysis of protonic acid doping of the emeraldine form of polyaniline, J. Phys. Chem. 92 (1988) 3657–3662.
[6] A.G. Macdiarmid, A.J. Epstein, Polyaniline: interrelationships between molecular weight, morphology, Donnan potential and conductivity, MRS Online Proc. Library Arch. 247 (1992).
[7] K. Neoh, E. Kang, K. Tan, Protonation of polyaniline films: effects of anion size and film structure, Polymer 35 (1994) 2899–2901.
[8] L. Wen, N. Kocherginsky, Doping-dependent ion selectivity of polyaniline membranes, Synth. Met. 106 (1999) 19–27.
[9] L. Wen, N. Kocherginsky, Coupled H+/anion transport through polyaniline membranes, J. Membr. Sci. 167 (2000) 135–146.
[10] P.K. Prajapati, R. Nimiwal, P.S. Singh, R.K. Nagarale, Polyaniline-co-epichlorohydrin nanoporous anion exchange membranes for diffusion dialysis, Polymer (2019).
[11] J.J. Alcaraz-Espinoza, A.E. Chávez-Guajardo, J.C. Medina-Llamas, C.S.A. Andrade, C.P. de Melo, Hierarchical composite polyaniline–(electrospun polystyrene) fibers applied to heavy metal remediation, ACS Appl. Mater. Interfaces 7 (2015) 7231–7240.
[12] N. Maity, A. Mandal, A.K. Nandi, High dielectric poly(vinylidene fluoride) nanocomposite films with MoS_2 using polyaniline interlinker via interfacial interaction, J. Mater. Chem. C 5 (2017) 12121–12133.
[13] P. Wang, K. Tan, E. Kang, K. Neoh, Preparation and characterization of semi-conductive poly(vinylidene fluoride)/polyaniline blends and membranes, Appl. Surf. Sci. 193 (2002) 36–45.
[14] L.F. Malmonge, G.D.A. Lopes, S.D.C. Langiano, J.A. Malmonge, J.M. Cordeiro, L.H.C. Mattoso, A new route to obtain PVDF/PANI conducting blends, Eur. Polym. J. 42 (2006) 3108–3113.
[15] Y. Zhang, L. Zou, B.P. Ladewig, D. Mulcahy, Synthesis and characterisation of superhydrophilic conductive heterogeneous PANI/PVDF anion-exchange membranes, Desalination 362 (2015) 59–67.
[16] R. Nagarale, G. Gohil, V.K. Shahi, Sulfonated poly(ether ether ketone)/polyaniline composite proton-exchange membrane, J. Membr. Sci. 280 (2006) 389–396.
[17] R. Nagarale, G. Gohil, V.K. Shahi, G. Trivedi, R. Rangarajan, Preparation and electrochemical characterization of cation-and anion-exchange/polyaniline composite membranes, J. Colloid Interface Sci. 277 (2004) 162–171.
[18] K.F. Hagesteijn, S. Jiang, B.P. Ladewig, A review of the synthesis and characterization of anion exchange membranes, J. Mater. Sci. 53 (2018) 11131–11150.
[19] Z. Yuan, H. Zhang, X. Li, Ion conducting membranes for aqueous flow battery systems, Chem. Commun. 54 (2018) 7570–7588.
[20] T. Xu, W. Yang, Tuning the diffusion dialysis performance by surface cross-linking of PPO anion exchange membranes—simultaneous recovery of sulfuric acid and nickel from electrolysis spent liquor of relatively low acid concentration, J. Hazard. Mater. 109 (2004) 157–164.
[21] R. Nagarale, G. Gohil, V.K. Shahi, Recent developments on ion-exchange membranes and electro-membrane processes, Adv. Colloid Interface Sci. 119 (2006) 97–130.
[22] J. Luo, C. Wu, Y. Wu, T. Xu, Diffusion dialysis of hydrochloride acid at different temperatures using PPO–SiO_2 hybrid anion exchange membranes, J. Membr. Sci. 347 (2010) 240–249.
[23] C. Wu, Y. Wu, J. Luo, T. Xu, Y. Fu, Anion exchange hybrid membranes from PVA and multi-alkoxy silicon copolymer tailored for diffusion dialysis process, J. Membr. Sci. 356 (2010) 96–104.
[24] X. Lin, E. Shamsaei, B. Kong, J.Z. Liu, T. Xu, H. Wang, Fabrication of asymmetrical diffusion dialysis membranes for rapid acid recovery with high purity, J. Mater. Chem. A 3 (2015) 24000–24007.
[25] T. Sata, Anti-organic fouling properties of composite membranes prepared from anion exchange membranes and polypyrrole, J. Chem. Soc., Chem. Commun. (1993) 1122–1124.
[26] D.L. Feldheim, C.M. Elliott, Switchable gate membranes. Conducting polymer films for the selective transport of neutral solution species, J. Membr. Sci. 70 (1992) 9–15.
[27] J. Yang, J. Hou, W. Zhu, M. Xu, M. Wan, Substituted polyaniline-polypropylene film composites: preparation and properties, Synth. Met. 80 (1996) 283–289.
[28] G. Tishchenko, J. Dybal, J. Stejskal, V. Kůdela, M. Bleha, E.Y. Rosova, G. Elyashevich, Electrical resistance and diffusion permeability of microporous polyethylene membranes modified with polypyrrole and polyaniline in solutions of electrolytes, J. Membr. Sci. 196 (2002) 279–287.
[29] H.S. Lee, J. Hong, Chemical synthesis and characterization of polypyrrole coated on porous membranes and its electrochemical stability, Synth. Met. 113 (2000) 115–119.
[30] S. Singh, K. Khulbe, T. Matsuura, P. Ramamurthy, Membrane characterization by solute transport and atomic force microscopy, J. Membr. Sci. 142 (1998) 111–127.
[31] B. Vyas, P. Ray, Preparation of nanofiltration membranes and relating surface chemistry with potential and topography: application in separation and desalting of amino acids, Desalination 362 (2015) 104–116.
[32] J. Mulder, Basic Principles of Membrane Technology, Springer Science & Business Media, 2012.
[33] C. Cheng, Z. Yang, J. Pan, B. Tong, T. Xu, Facile and cost effective PVA based hybrid membrane fabrication for acid recovery, Sep. Purif. Technol. 136 (2014) 250–257.
[34] D.M. Stachera, R.F. Childs, A.M. Mika, J.M. Dickson, Acid recovery using diffusion dialysis with poly(4-vinylpyridine)-filled microporous membranes, J. Membr. Sci. 148 (1998) 119–127.
[35] T. Xu, W. Yang, Sulfuric acid recovery from titanium white (pigment) waste liquor using diffusion dialysis with a new series of anion exchange membranes—static runs, J. Membr. Sci. 183 (2001) 193–200.
[36] B. Han, J. Pan, S. Yang, M. Zhou, J. Li, A. Sotto Díaz, B. Van der Bruggen, C. Gao, J. Shen, Novel composite anion exchange membranes based on quaternized polyepichlorohydrin for electromembrane application, Ind. Eng. Chem. Res. 55 (2016)

7171–7178.
[37] S. Cho, M. Kim, J.S. Lee, J. Jang, Polypropylene/polyaniline nanofiber/reduced graphene oxide nanocomposite with enhanced electrical, dielectric, and ferroelectric properties for a high energy density capacitor, ACS Appl. Mater. Interfaces 7 (2015) 22301–22314.
[38] D.L. Pavia, G.M. Lampman, G.S. Kriz, J.A. Vyvyan, Introduction to Spectroscopy, Cengage Learning, 2008.
[39] M.C. Lukowiak, S. Wettmarshausen, G. Hidde, P. Landsberger, V. Boenke, K. Rodenacker, U. Braun, J.F. Friedrich, A.A. Gorbushina, R. Haag, Polyglycerol coated polypropylene surfaces for protein and bacteria resistance, Polym. Chem. 6 (2015) 1350–1359.
[40] Q. Li, X. Pan, C. Hou, Y. Jin, H. Dai, H. Wang, X. Zhao, X. Liu, Exploring the dependence of bulk properties on surface chemistries and microstructures of commercially composite RO membranes by novel characterization approaches, Desalination 292 (2012) 9–18.
[41] R. Ansari, M. Keivani, Polyaniline conducting electroactive polymers thermal and environmental stability studies, J. Chem. 3 (2006) 202–217.
[42] D. Kumar, R. Chandra, Thermal behaviour of synthetic metals, Polyanilines (2001).
[43] T. Sata, T. Yamaguchi, K. Matsusaki, Effect of hydrophobicity of ion exchange groups of anion exchange membranes on permselectivity between two anions, J. Phys. Chem. 99 (1995) 12875–12882.
[44] Y. Marcus, Ionic radii in aqueous solutions, Chem. Rev. 88 (1988) 1475–1498.
[45] H. Ma, Hydration structure of $Na+$, $K+$, $F-$, and $Cl-$ in ambient and supercritical water: a quantum mechanics/molecular mechanics study, Int. J. Quantum Chem. 114 (2014) 1006–1011.
[46] Y. Marcus, Thermodynamics of solvation of ions. Part 5. —Gibbs free energy of hydration at 298.15 K, J. Chem. Soc., Faraday Trans. 87 (1991) 2995–2999.
[47] Y. Wu, C. Wu, Y. Li, T. Xu, Y. Fu, PVA–silica anion-exchange hybrid membranes prepared through a copolymer crosslinking agent, J. Membr. Sci. 350 (2010) 322–332.
[48] A.N. Mondal, C. Cheng, Z. Yao, J. Pan, M.M. Hossain, M.I. Khan, Z. Yang, L. Wu, T. Xu, Novel quaternized aromatic amine based hybrid PVA membranes for acid recovery, J. Membr. Sci. 490 (2015) 29–37.
[49] J. Pan, Y. He, L. Wu, C. Jiang, B. Wu, A.N. Mondal, C. Cheng, T. Xu, Anion exchange membranes from hot-pressed electrospun QPPO–SiO_2 hybrid nanofibers for acid recovery, J. Membr. Sci. 480 (2015) 115–121.
[50] K. Emmanuel, C. Cheng, B. Erigene, A.N. Mondal, M.M. Hossain, M.I. Khan, N.U. Afsar, G. Liang, L. Wu, T. Xu, Imidazolium functionalized anion exchange membrane blended with PVA for acid recovery via diffusion dialysis process, J. Membr. Sci. 497 (2016) 209–215.
[51] D.-H. Kim, J.-H. Park, S.-J. Seo, J.-S. Park, S. Jung, Y.S. Kang, J.-H. Choi, M.-S. Kang, Development of thin anion-exchange pore-filled membranes for high diffusion dialysis performance, J. Membr. Sci. 447 (2013) 80–86.
[52] D.-H. Kim, H.-S. Park, S.-J. Seo, J.-S. Park, S.-H. Moon, Y.-W. Choi, Y.S. Jiong, D.H. Kim, M.-S. Kang, Facile surface modification of anion-exchange membranes for improvement of diffusion dialysis performance, J. Colloid Interface Sci. 416 (2014) 19–24.